White Rose
university consortium
Universities of Leeds, Sheffield & York

eprints@whiterose.ac.uk
https://eprints.whiterose.ac.uk/

Accelerated spreading of inviscid droplets prompted by the yielding of strongly elastic interfacial films

Emily James[1], Suparit Tangparitkul[1], Anju Brooker[2], Carlos Amador[2], Andrew Graydon[2], Mauro Vaccaro[2], Olivier J. Cayre,[1] Timothy N. Hunter[1] and David Harbottle[*1]

[1]School of Chemical and Process Engineering, University of Leeds, Leeds, UK
[2]Procter & Gamble Ltd., Whitley Road, Newcastle, Tyne and Wear, UK

Abstract

The complexity associated with droplets spreading on surfaces has attracted significant interest for several decades. Sustained activity results from the many natural and manufactured systems that are reliant on droplet-substrate interactions and spreading. Interfacial shear rheology and its influence on the dynamics of droplet spreading has to date received little attention. In the current study, saponin β-aescin was used as an interfacial shear rheology modifier, partitioning at the air-water interface to form a strongly elastic interface (G'/G" ~ 6) within 1 min aging. The droplet spreading dynamics of Newtonian (water, 5 wt% ethanol, 0.0015 wt% N-dodecyl β-D-glucopyranoside) and non-Newtonian (xanthan gum) fluids were shown to proceed with a time-dependent power-law dependence of ~ 0.50 and ~ 0.10 (Tanner's law) in the inertial and viscous regimes of spreading, respectively. However, water droplets stabilized by saponin β-aescin were shown to accelerate droplet spreading in the inertial regime with a depreciating time-dependent power-law of 1.05 and 0.61, eventually exhibiting a power-law dependence of ~ 0.10 in the viscous regime of spreading. The accelerated rate of spreading is attributed to the potential energy as the interfacial film yields as well as relaxation of the crumpled interfacial film during spreading. Even though the strongly elastic film ruptures to promote droplet spreading, interfacial elasticity is retained enhancing the dampening of droplet oscillations following detachment from the dispensing capillary.

Introduction

Spreading droplets are important in many industries including paints, coatings, agrochemicals and lubrication to name just a few.[1] The energy associated with a droplet spreading on a solid in air is given by, $-\frac{dG}{dA} = \gamma_{S/G} - (\gamma_{S/L} + \gamma_{L/G})$, where (γ_{xy}) is the interfacial tension between three phases, S = solid, L = liquid and G = gas. When combined with the well-known Young's equation $(\cos\theta = \frac{\gamma_{S/G} - \gamma_{S/L}}{\gamma_{L/G}})$, the energy associated with droplet spreading yields

$$-\frac{dG}{dA} = \gamma_{L/G}(cos\theta - 1) \geq 0. \qquad (1)$$

Droplet spreading in air has been extensively studied[2] and several models including Tanner (Eq. 2)[3], Seaver and Berg[4], and de Gennes[5] have been proposed to describe the droplet spreading dynamics. Tanner's spreading theory is widely reported for viscous liquids spreading on hydrophilic surfaces, with the hydrodynamic spreading radius (r) dependent on the initial droplet radius R', the surface tension γ, the fluid viscosity μ, and the spreading time t [3, 6]

$$\frac{r}{R'} \sim \left(\frac{\gamma t}{\mu R'}\right)^{1/10}. \qquad (2)$$

While most fluids can reasonably be described by Tanner's law, Sawicki et al. showed discrepancies for low viscosity poly(dimethyl siloxane) (PDMS) oils.[7] Such divergence was suggested to relate to the interfacial viscosity being significantly lower than the bulk fluid viscosity, resulting from differences in molecular orientation at the interface.

The dynamics of inviscid droplet spreading exhibit two distinct regimes; the first phase of spreading is commonly termed inertial spreading and progresses at a rate of $r \sim t^{0.5}$, [8-9] while the second phase is described as viscous spreading and the three-phase contact line moves as a function of $r \sim t^{0.1}$, i.e. Tanner's law. The viscous regime is limited by droplet viscosity[9], with

the characteristic time of spreading (Eq. 3) used to describe the transition from inertial to viscous spreading[10]

$$\tau \sim \left(\frac{\rho \gamma R'}{\mu^2}\right)^{1/8} \sqrt{\frac{\rho R'^3}{\gamma}} \qquad (3)$$

where ρ is the droplet density.

Table 1 summarizes the effect of several fluid and surface properties on the spreading dynamics of mostly inviscid droplets. In addition to those commonly studied properties, there are many other factors that have been shown to influence spreading dynamics including drop shape[11], surface roughness[12], temperature[13-14], complex and soft surfaces[15-16], electro-wetting[17-18] and droplet impact velocity.[19]

Table 1. The effect of physicochemical properties on the spreading dynamics of droplets. The spreading exponents in the inertial and viscous regimes are represented as n′ and n″, respectively.

Parameter	Impact on spreading	Spreading exponent
Fluid viscosity (droplet)	General observation: Increased viscosity decreases the droplet spreading rate.	n″ ~ 0.15, μ = 11.5 – 1120 mPa.s [9] n′ ~ 0.5, μ = 1 – 10.7 mPa.s [20] n′ ~ 0.5 then n″ ~ 0.1, μ = 1 – 1000 mPa.s [10] 0.3 < n′ < 0.5 then 0.1 < n″ < 0.125, μ = 1 – 60.1 mPa.s [21] 0.1 < n″ < 0.2, μ = 35.5 – 109 mPa.s [19] n′ ~ 0.5 then n″ ~ 0.1, μ = 1 – 1412 mPa.s [22] 0.12 < n″ < 0.18, μ = 1.34 – 50000 mPa.s [23] 0.030 < n′ < 0.085 then 0.073 < n″ < 0.109, μ = 20 – 1150 mPa.s [24]
Surface wettability	General observation: Aqueous droplets on hydrophilic (water-wet) surfaces – reduced substrate hydrophilicity decreases the droplet spreading rate.	n′ = 0.5, θ = 0 – 115° [9] n′ ~ 0.5 then 0.06 < n″ < 0.1, θ = 0 – 50° [13] 0.25 < n′ < 0.5, θ = 30 – 180°, 3 – 180° [20] 0.3 < n′ < 0.5 then n″ ~ 0.1, θ = 0 – 112° [21] n′ ~ 0.5, θ = 0 – 115° [25] 0.1437 < n′ < 0.2785, θ = 0 – 36.8° [26]
Initial drop size	General observation: Droplets with a size below the capillary length spread at a rate n″ ~ 0.1. R′ = radius	0.5 < n′ < 1 then 0.1 < n″ < 0.2, R′ 0.37 – 0.82 mm [9] n′ ~ 0.5, R′ 0.22 – 0.78 mm [20] n′ ~ 0.5 then n″ ~ 0.1, R′ 1.2 – 2.7 mm [10] 0.44 < n′ < 0.53, R′ 0.5 – 1.2 mm [21] 0.14 < n″ < 0.2, R′ 10 μm – 2.5 mm [19] 0.073 < n″ < 0.141, R′ 1.24 – 1.34 mm [24] 0.1 < n″ < 0.13, R′ 0.57 – 1.51 mm [12]

Surface tension	General observation: Decrease in surface tension increases droplet spreading rate. Using surfactants either: a) increase spreading dynamics (trisiloxanes (TS)) or b) decrease spreading dynamics (docusate (AOT), CTAB, SDS).	TS $0.16 < n'' < 1$, AOT $n'' \sim 0.1$ [27] $0.001 < n'' < 0.06$ [28] $0.053 < n'' < 0.09$ [29] pure liquids $n' \sim 0.5$ then $n'' \sim 0.1$, [22] surfactant $n' \sim 0.5$ then $n'' < 0.1$ [22] $0.053 < n'' < 0.1$ [30] TS $0.015 < n' < 0.23$ then $0.38 < n'' < 0.58$ [23] $0.099 < n'' < 0.137$ [24]

Of particular interest in the current study is the contribution from surface elasticity which can be influenced by surface active species partitioning at the liquid-liquid interface.[31-34] To the authors' knowledge, interfacial effects on the spreading dynamics of droplets are rarely explored except for surfactant systems, with particular focus given to changes in surface tension. Generally, surfactants reduce the equilibrium three-phase contact angle and increase the solid-liquid contact area. However, the rate of droplet spreading is slightly retarded as the creation of new interfacial area is significantly faster than the diffusion transport of surfactants to the interface,[35] hence surface tension gradients are established during droplet spreading leading to Marangoni flows.[36]

However, few studies have considered the influence of surface shear elasticity on droplet spreading dynamics. Leiske et al. considered the contribution of surface elasticity on the mobility of droplets residing on a sliding substrate.[37] The authors selected four insoluble surfactants to produce varying degrees of surface elasticity, as the insoluble nature of these surfactants was a determinant property to generate surface shear elasticity. The authors evidenced that the motion of a droplet on a sliding substrate was influenced by the surface shear elasticity and not solely by the surface tension. For the most rigid interface the authors observed compression of the droplet interface and the formation of an interfacial skin which eventually ruptured to promote droplet spreading.

To advance our understanding of the effects of interfacial rheology on droplet spreading dynamics, in the current study, β-aescin was chosen as an interfacial rheology modifier. The molecular structure of β-aescin (Fig. 1) is highly polycyclic and favors the formation of strongly elastic films at the air-water interface.[38] The research objective was to assess the contribution of interfacial shear elasticity on droplet spreading dynamics.

Materials and Experimental Methods

Saponin β-aescin (purity 95 %, Mw 1101.2 g/mol) a triterpenoid monodesmosidic glycoside, was purchased from MP Biomedicals (UK). A non-ionic surfactant, N-Dodecyl *β*-D-glucopyranoside (DG) (purity 98 %, Mw 320 g/mol), and xanthan gum (XG) (Mw 4.5MDa) were purchased from Sigma Aldrich (UK). Silicon wafers were used as the wetting substrate and were purchased from Silicon Valley Microelectronics (USA). The properties of the silicon wafers were: Type P, dopant: boron, orientation <100>, resistivity 10 – 20 ohm.cm and thickness 525 ± 25 μm. Ultrapure Milli-Q water was used in all experiments with a minimum resistivity of 18.2 MΩ·cm. Ethanol (purity 99.96% A.C.S. grade, VWR) and PDMS (Alfa Aesar, USA) with a nominal viscosity of 1000 mPa·s were used as received.
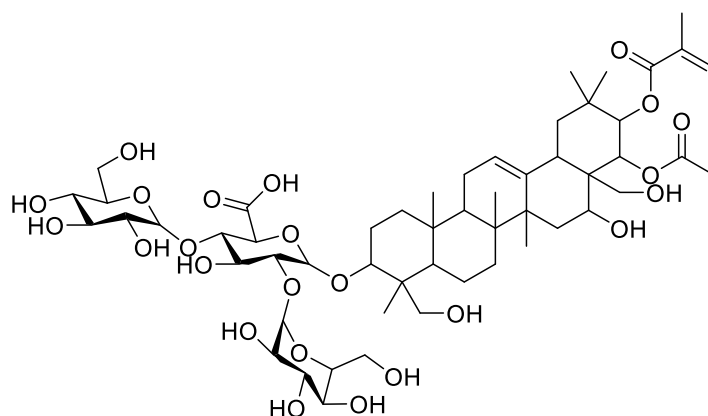

Figure 1. General molecular structure of β-aescin.

Surface tension: The dynamic surface tension of a droplet was measured using a pendant droplet analyzer (Theta T200, Biolin Scientific, Sweden). A droplet of ~8 µL was generated at the blunt tip of a 22 G stainless steel (SS) needle at 2 µL/s using an automatic dispenser. Prior to each measurement, the SS needle was cleaned using ethanol and dried with nitrogen. The surface tension was determined from droplet shape analysis, with the Theta software executing an edge-detection routine. The β-aescin concentration in Milli-Q water was varied between 5 $\times$ 10^{-5} wt% and 0.5 wt%. The surface tension was measured for 0.83 h to ensure that the steady-state condition was attained. The influence of droplet evaporation was minimized by increasing the relative humidity in the quartz cuvette and sealing the measurement cell using Parafilm. Small changes in the droplet volume were also compensated by activating the automatic evaporation tool in the Theta software. The feedback loop ensured that the droplet volume was maintained by automatically injecting fluid when the droplet volume diverged by 1 %.

Prior to generating the water droplet, the imaging software was triggered to capture the initial adsorption dynamics. For surface tension measurements the image capture rate was set to 2 fps.

Droplet spreading: Even though the Theta tensiometer had a maximum frame rate of 2,500 fps, the frame rate was too slow to fully capture the detail of inviscid droplet spreading. Therefore, a high speed camera (Photron FASTCAM SA5, Photron Ltd., Japan) was used to record droplet spreading at 10,000 fps. The high speed camera was positioned perpendicular to the Theta tensiometer and slightly elevated ($< 2°$) above the spreading surface. Two LED lights were positioned in front of the quartz cuvette either side of the camera to provide sufficient illumination of the spreading droplet. 10 µL droplets were instantaneously produced at the blunt-tip of a 22 G SS needle. The needle tip was positioned 5.5 mm from the spreading substrate, with the droplet apex (lower edge) ~ 3.5 mm from the spreading substrate. Depending on the system, the droplet was held in position for a pre-determined time to ensure that the interfacial properties (surface tension, surface shear elasticity) had approached near steady-

state. The droplet hold time for water + β-aescin was 5 min. Once the droplet had aged, the droplet was lowered towards the underlying substrate at 10 mm/min whilst remaining attached to the SS needle. The rate of droplet approach (0.17 mm/s) was maintained beyond droplet contact with the spreading substrate. Since droplet spreading occurred over a few hundredths of a second, this mechanical motion had little effect on the spreading rate, and the droplet always detached from the SS needle during spreading. The captured images were analysed using ImageJ software to measure the droplet spreading diameter and droplet height (centreline) as a function of time. Prior to each measurement, the silicon wafers were cleaned by soaking the substrates in Piranha solution for 2 h, thoroughly rinsing with Milli-Q water and dried with nitrogen.

Fluid and interfacial shear rheology: The viscosity of β-aescin solutions and the interfacial shear rheology of the air-water interface were measured using a Discovery Hybrid Rheometer (DHR-2) (TA Instruments, UK). Equivalent β-aescin concentrations as those discussed for surface tension measurements were considered. The concentric cylinder geometry was used to measure the viscosity of the β-aescin solutions, and the geometry was chosen to minimize the surface area to volume ratio, thus ensuring that any contribution from interfacial rheology on the bulk viscosity was negligible. The shear viscoelasticity of the air-aqueous (water + β-aescin) interface was measured using the Double Wall Ring (DWR) geometry. The method of cleaning and set-up have been described in detail elsewhere.[34] It should be noted that the instrument was calibrated using precision mapping and the bearing mode set to soft. The geometry was positioned at the air-aqueous interface and a pre-shear protocol ($\dot{\gamma}$ = 170 s^{-1} for 3 min) initiated to ensure that the start condition for each experiment remained constant. The time-dependent viscoelasticity was measured by oscillating the DWR at constant strain, 0.05%, and constant frequency, 1 Hz. A strain dependent sweep verified that the oscillation strain remained in the linear viscoelastic region. The G' (elastic) and G'' (viscous) moduli were

measured for 30 min and to minimize the effect of solvent evaporation a Teflon cap was placed over the DWR Delrin trough. All rheology experiments were completed at T = 20 °C.

Results and Discussion

The spreading of water (inviscid) droplets is shown in Fig. 2. The two distinct regimes can be identified as inertial and viscous spreading, with the exponent of spreading decreasing from 0.50 to 0.10, the latter in good agreement with Tanner's law. Using Eq. 3, the characteristic time of spreading was calculated to be 8×10^{-3} s, which identifies the onset of the transition from inertial to viscous spreading, see Fig. 2. Three repeats are shown in Fig. 2 and confirm good reproducibility of the spreading dynamics. The spreading exponents for each experiment are shown inset.

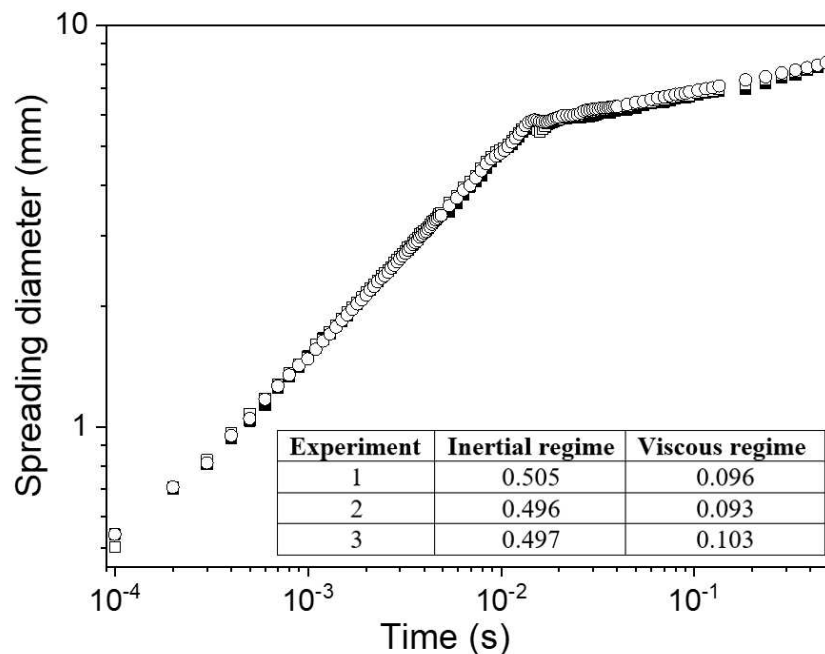| Experiment	Inertial regime	Viscous regime
1	0.505	0.096
2	0.496	0.093
3	0.497	0.103

Figure 2. Spreading dynamics of three water droplets deposited on a hydrophilic silicon substrate.

Surface tension: The dynamic surface tension of water + β-aescin was measured to determine the minimum adsorption time required to reach steady-state. Fig. 3a shows the dependence of β-aescin concentration on surface tension, with concentrations less than 5×10^{-3} wt% resulting

in negligible changes to the surface tension (γ_{water} = 72.3 mN/m). At concentrations ≥ 5 × 10^{-3} wt%, the surface tension was observed to progressively decrease with increasing β-aescin concentrations up to 5 × 10^{-2} wt%. At higher β-aescin concentrations the adsorption dynamics and apparent surface tension was independent of concentration, i.e. beyond the critical micelle concentration (CMC) of β-aescin.

The apparent surface tension isotherm is shown in Fig. 3b. Three additional β-aescin concentrations were also measured such that the CMC could be determined, CMC = 0.2 mM (0.022 wt%), in reasonable agreement with the range of CMCs previously reported by Pekdemir et al.[39] CMC = 0.78 mM and Stoyanov et al.[38] CMC = 0.071 mM. The order of magnitude difference in the reported CMC may result from differences in the molecular composition and purity of the β-aescin, which is reasonable since β-aescin is a naturally sourced product. The variability in reported CMC values might also be attributed to a non-surface tension force. As will be discussed below, β-aescin forms strongly elastic interfaces and the effect of the resulting deviatoric stresses can deform the droplet, leading to apparent changes in the measured surface tension.[40] As such, we refer to the surface tension as an apparent surface tension.

The slope of the apparent surface tension isotherm can by analysed using the Gibbs equation ($\frac{-d\gamma}{RT} = \Gamma \, d\ln C$) to determine the maximum adsorption of β-aescin (Γ_{max}) at the air-water interface. In the Gibbs equation, Γ represents the excess solute per unit area at the interface, R the universal gas constant, T the temperature, γ the surface tension, and C the bulk concentration of β-aescin in Milli-Q water. Γ_{max} for β-aescin at the air-water interface was calculated to be 6.59 × 10^{-6} mol/m^2. From the surface excess the area per molecule (A_i) can be calculated using $A_i = (1/\Gamma_{max}N_A)$, where N_A is Avogadro's constant, hence, for the β-aescin used in the current study the area per molecule was 0.26 nm^2. Stanimirova et al.[41] used

molecular dynamics simulations to elucidate the interfacial ordering of β-aescin (air-water) and showed two preferred orientations, i) lay-on configuration (i.e. parallel to the interface) $A_i \sim$ 0.75 nm^2, and ii) end-on configuration (i.e. perpendicular to the interface) $A_i \sim$ 0.26 nm^2. The latter configuration is in good agreement with the calculated area per molecule, hence it is most likely that the end-on configuration is the preferential orientation of β-aescin at the air-water interface.
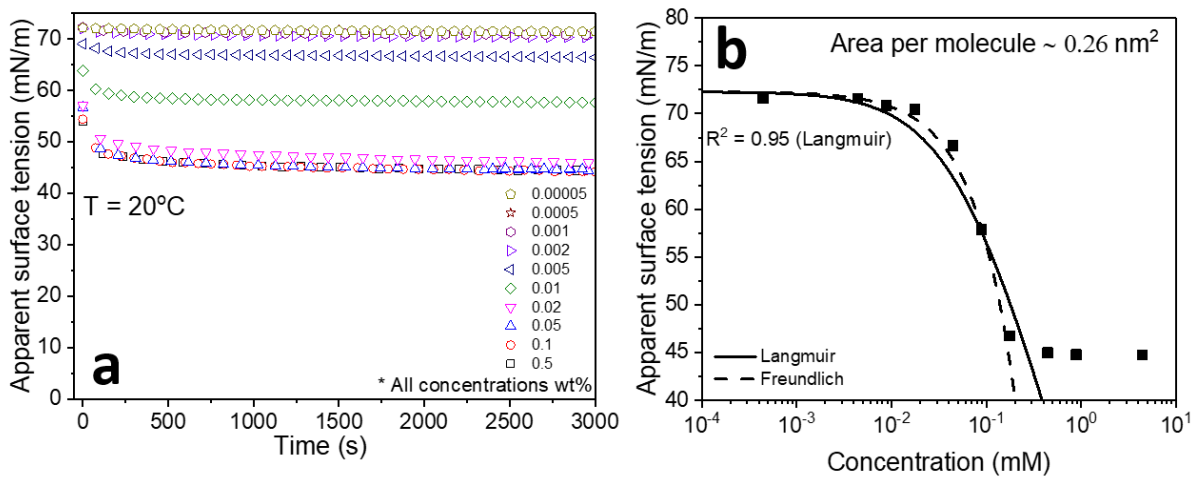

Figure 3. a) Dynamic surface tension of water droplets with increasing concentrations of β-aescin. b) Apparent equilibrium surface tensions as a function of the β-aescin concentration.

The apparent surface tension isotherm was fitted to a Langmuir model ($\gamma = \gamma_a + RT\Gamma_{max}\ln(\frac{1}{1+KC})$) with a coefficient of determination equal to 0.95. A slightly better fit to the experimental data was observed using the empirical Freundlich isotherm which may suggest that the adsorbed β-aescin film is slightly heterogeneous, although this has not been confirmed.

Fluid and interfacial shear rheology: The primary objective of this study was to isolate the contribution of interfacial shear rheology on droplet spreading, hence a critical concentration of β-aescin was first determined, such that the effect of β-aescin on interfacial rheology was significant while changes to bulk fluid viscosity were negligible. The bulk viscosities of β-

aescin solutions over the concentration range 5×10^{-4} wt% to 0.5 wt% are shown in Fig. 4a. At β-aescin concentrations $\leq 5 \times 10^{-3}$ wt%, the fluid can be considered to behave as a Newtonian fluid with a measured viscosity equal to water. At higher β-aescin concentrations the fluid becomes non-Newtonian (shear thinning), with a fluid viscosity slightly exceeding water. For example, at a β-aescin concentration of 0.01 wt% and a shear rate of 40 s^{-1}, the relative viscosity ($\frac{\mu_\beta}{\mu_W}$) was increased by 12% and demonstrated weakly shear thinning behaviour, power-law index = 0.84. The degree of fluid shear thinning was shown to increase slightly at higher β-aescin concentrations, although the fluid rheology displayed little variation at concentrations beyond the CMC.

While the exact shear rate during droplet spreading is not known, the shear rate (γ_0) at droplet impact can be approximated by $\gamma_0 = \frac{U_0}{D_0}$, where U_0 and D_0 are the droplet impact velocity and droplet diameter, respectively.[19] In the current study the droplet shear rate at impact was ~ 0.05 s^{-1}. Based on the relative differences in spreading and impact velocities, it is expected that the droplet shear rate during spreading greatly increases. Hence, the difference in viscosity between Milli-Q water and the shear rate dependent viscosity of 0.01 wt% β-aescin solution can be considered negligible. To assess the importance of equivalent shear thinning behavior on droplet spreading dynamics, a comparative study using xanthan gum was also considered. Xanthan gum was chosen due to its ability to structure in solution and consequently affect the bulk fluid viscosity while showing negligible surface activity (measured to be 71.5 mN/m up to 0.05 wt%), thus not affecting the interfacial shear rheology.

For equivalent β-aescin concentrations (bulk rheology), the shear viscoelastic properties of the air-water interface were measured to elucidate the time-dependent build-up of both the viscous (G'') and elastic moduli (G'). At β-aescin concentrations lower than 5×10^{-3} wt%, the interface remained purely viscous with no measurable elasticity. This is in good agreement with the

negligible changes in air-water surface tension at low β-aescin concentrations (Fig. 3a), thus suggesting sparse coverage of β-aescin molecules at the air-water interface. Increasing the β-aescin concentration led to the onset of a measureable elasticity (c = 5 × 10^{-3} wt%), while at higher β-aescin concentrations strongly elastic interfacial films were formed and could be considered solid-like (i.e. $G' > G''$). The critical β-aescin concentration required to develop a solid-like interfacial film was found to be 0.01 wt%, but this also corresponded to the onset of a weakly shear thinning fluid, see Fig. 4a. Following the pre-shear protocol, the aging time required for the air-water interface to become solid-like was less than 30 s (c = 0.01 wt%), and became almost instantaneous (few seconds) at higher β-aescin concentrations. For 0.01 wt% β-aescin in water, the G'/G'' ratio at 5 min aging was ~ 10, confirming the strongly elastic nature of the formed interfacial film.

At 0.01 wt% β-aescin, even though the relative viscosity of the bulk fluid had increased by 12% (compared to water at a shear rate of 40 s^{-1}), a significant change in the interfacial shear rheology was observed, transitioning from a purely viscous (water only at t = 0) to a solid-like interface that was sufficiently strong to induce an apparent interfacial yield stress of ~ 1.7 x 10^5 Pa. The 2D yield point of the interfacial film was measured via an oscillation stress ramp[42] (Fig. S1) following 5 min aging. The critical stress at $G' = G''$ was converted to an apparent yield stress by including the interfacial film thickness (5 nm), which was taken to be equivalent to a monolayer thick.[38, 43]
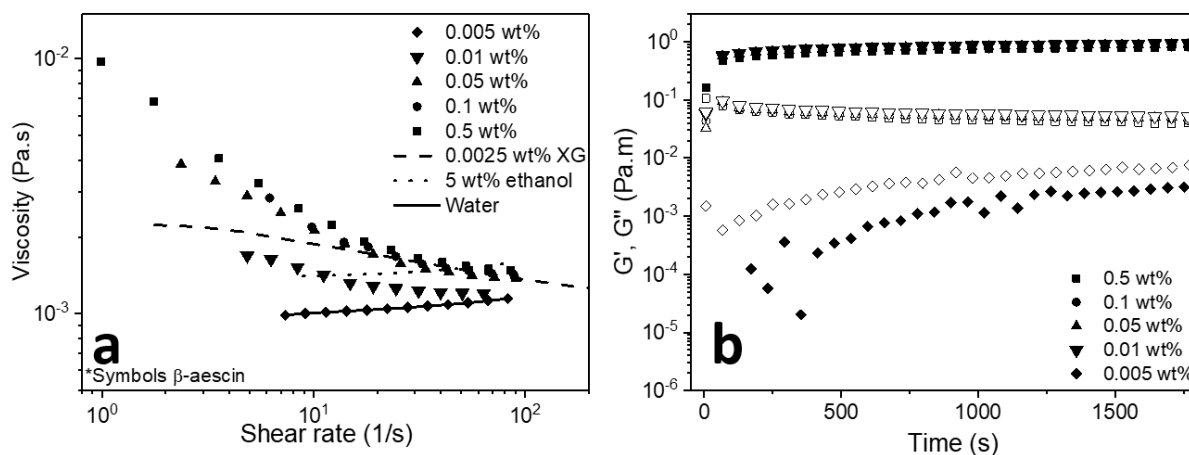
Figure 4. a) Fluid viscosity as a function of the β-aescin concentration. Lines represent the rheology of water (solid), water + 5 wt% ethanol (dotted) and water + 0.0025 wt% xanthan gum solution (dashed). b) Interfacial shear viscoelasticity of β-aescin films at the air-water interface as a function of the β-aescin concentration and interfacial aging time. Open symbols = G', closed symbols = G''. Oscillation rheology conducted using constant strain, 0.05 % and constant frequency, 1 Hz. All experiments were conducted at T = 20 ºC.

Droplet spreading: The spreading dynamics of inviscid droplets without and with interfacial shear elasticity have been compared. The rheology data confirmed that the critical β-aescin concentration to generate substantial interfacial shear elasticity but weakly modify the fluid rheology was 0.01 wt%, hence this concentration was considered for the comparison study. Fig. 5 is a series of images depicting the time-dependent spreading or pure water and water + 0.01 wt% β-aescin droplets. For a water droplet (Fig. 5a), following contact with the spreading substrate, rapid expansion of the contact area was observed with the three-phase contact line moving at ~ 400 mm/s. As the droplet continues to spread, a fluid 'neck' forms between the spreading droplet and the fluid pinned at the tip of the capillary. The fluid neck was observed to rapidly thin, eventually destabilising to separate the spreading droplet from the liquid pinned at the tip of the dispensing capillary.
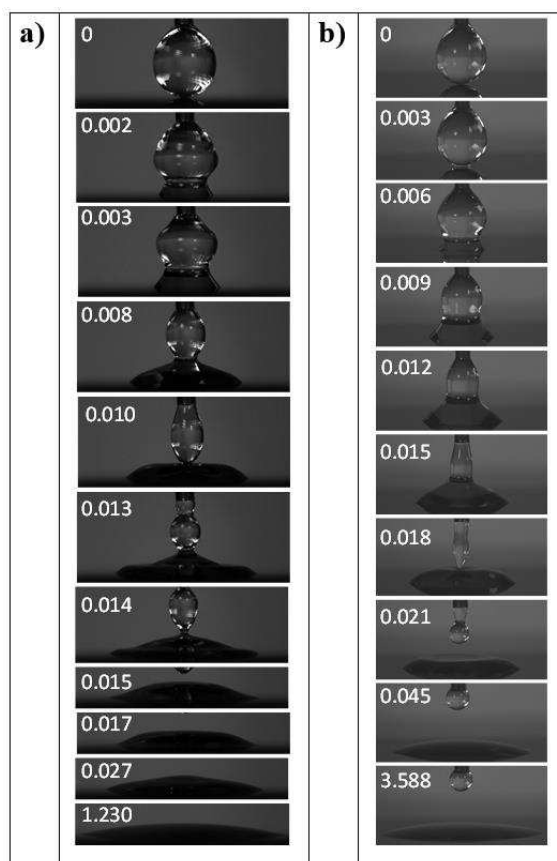
Figure 5. Time-dependent sequence of a) water droplet and b) 0.01 wt% β-aescin droplet spreading on a hydrophilic silicon substrate. Droplet spreading times (s) shown inset.

Fig. 5b shows a similar time sequence for the 0.01 wt% β-aescin droplet spreading on a hydrophilic silicon substrate. The spreading droplet again detaches from the liquid retained at the tip of the dispensing capillary, although it is clear from the image sequence that the formation of the fluid neck and eventual pinch-off is affected by interfacial rigidity. Indeed, the fluid neck exhibits less deformation than the pure water droplet, retaining an almost cylindrical shape before eventually pinching-off at the apex of the spreading droplet (t ~ 0.018 s).

The spreading dynamics of pure water and water + 0.01 wt% β-aescin are compared in Fig. 6. Firstly, the spreading dynamics of both fluids exhibit inertial and viscous regimes. While the

spreading of water obeys the classical spreading exponents, $t^{0.5}$ and $t^{0.1}$, the water + 0.01 wt% β-aescin droplet appears to exhibit two spreading exponents in the 'conventional' inertial spreading regime. Between t = 0 and t = 5×10^{-4} s the droplet spreads with an exponent $t^{1.05}$, slightly reducing to an exponent of $t^{0.61}$ until the viscous spreading regime is reached and the droplet continues to spread with an exponent of $t^{0.11}$. The spreading exponents for all fluids are summarized in Table 2. Based on the measured spreading exponents, the presence of β-aescin at the air-water interface accelerates the rate of inertial droplet spreading. To elucidate the contribution of strong interfacial elasticity to accelerated spreading, three other fluids were considered for comparison i) 5 wt% ethanol solution, ii) 0.0015wt% glucopyranoside (DG) solution, and iii) 0.0025 wt% xanthan gum (XG) solution. The ethanol and DG fluids were specifically chosen so that the surface tension was 57 mN/m at 20 °C, equivalent to the surface tension of the 0.01 wt% β-aescin solution. Both fluids were purely viscous (shear independent viscosity), although the DG surfactant was selected to mimic the presence of surface active molecules without developing interfacial shear elasticity. XG was selected at the specific concentration to mimic the weakly shear thinning behavior of the β-aescin solution (Fig. 4a) with no interfacial shear elasticity. As shown in Fig. 6 and summarized in Table 2, all droplets, except β-aescin, were observed to spread with exponents equivalent to water. Hence, the slight reduction in surface tension, increased fluid viscosity and shear thinning behaviour of the fluid were found to have minimal effect on the spreading exponents, and thus the accelerated inertial spreading of the water + β-aescin droplet can be attributed to the strongly elastic interface.
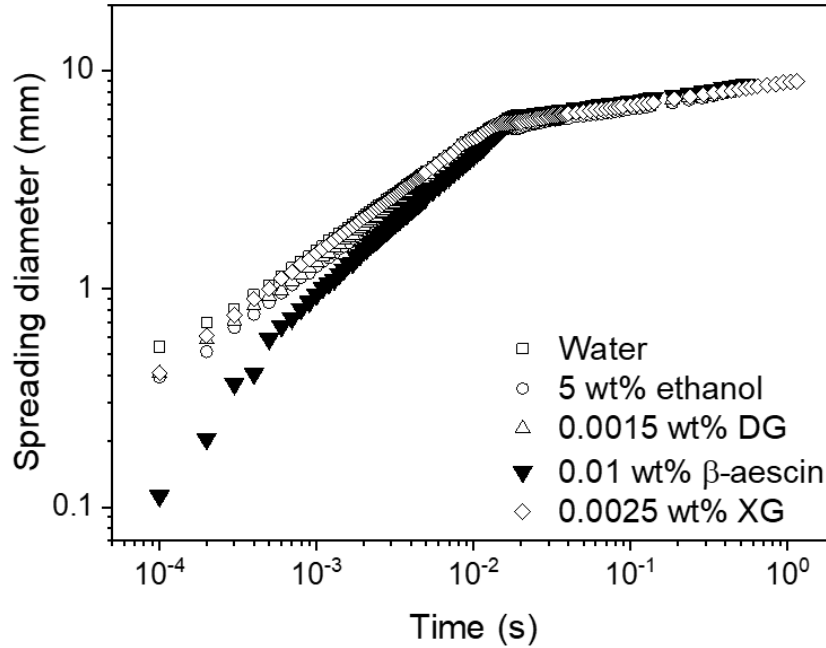
Figure 6. Comparison of droplet spreading dynamics in the inertial and viscous regimes. The droplet volume and the droplet-substrate approach velocity remained constant at 10 µL and 10 mm/min, respectively. The β-aescin and DG droplets were aged for 5 min prior to initiating droplet approach.

From Fig. 6, it can be seen at t = 10^{-4} s (first captured image of droplet spreading), the initial spreading diameters are equivalent for all droplets with a purely viscous interface (within error), but greatly exceed the initial spreading diameter of the water + 0.01 wt% β-aescin droplet. This variation highlights that the mechanism of droplet spreading is likely different when the droplet interface is strongly elastic. The interfacial shear rheology data confirmed that the interface stabilized by β-aescin exhibits a yield stress, which is able to initially resist droplet spreading upon droplet-substrate contact. However, as the droplet continues to descend towards the substrate, the droplet becomes sufficiently deformed such that the β-aescin stabilized interfacial film ruptures to initiate droplet spreading. This is in contrast to the droplets whose interfaces are purely viscous and instantaneously spread when contacting the substrate. Hence, the rate of droplet spreading is initially retarded by the yield stress interface but once

the interfacial film ruptures the droplet spreading rate is accelerated compared to fluids with no interfacial shear elasticity.

The contribution from the shear elastic interface on droplet spreading is evidenced by the interfacial crumpling at t = 0.0025 s (Fig. 7), which is induced by the negative curvature of the droplet compressing the interfacial material. As such, during droplet spreading the elastic interface drives minimization of the negative curvature and alleviates interfacial compression. It is likely that this phenomenon combined with the potential energy liberated at the point of interfacial film rupture contribute to the enhanced rate of droplet spreading in the inertial regime.
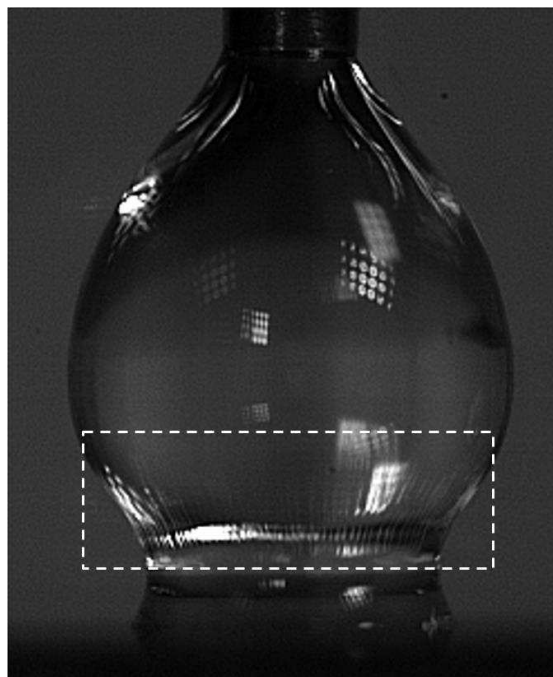

Figure 7. Observed interfacial crumpling of a 0.01 wt% β-aescin stabilized droplet during spreading.

Table 2. Droplet spreading exponents in the inertial and viscous regimes.

Fluid	Inertial regime		Viscous regime
0.01 wt% β-aescin	1.05 ± 0.07	0.61 ± 0.02	0.11 ± 0.009
Water	0.50 ± 0.002		0.10 ± 0.005
0.0015 wt% DG	0.52 ± 0.010		0.11 ± 0.005
5 wt% ethanol	0.51 ± 0.001		0.11 ± 0.008
0.0025 wt% XG	0.51 ± 0.009		0.10 ± 0.003

Droplet oscillations: Differences in the damped oscillations of detached droplets were also observed. These oscillations can be modelled by a simple damped oscillation, $A(t) = A_0 \exp(-\beta t) \sin(\omega t + \psi)$, where A(t) is the droplet peak height, A_0 the initial droplet height, ω the frequency of oscillation, ψ the phase shift and β the dampening coefficient.[44]

Fig. 8 compares the damped oscillation of water droplets without and with 0.01 wt% β-aescin. With the droplets detached from the dispensing capillary the two data sets were superimposed such that the minimum during the first oscillation cycle was aligned (A(t) = 3.5 mm when t = 0.0075 s). With 0.01 wt% β-aescin, the droplet oscillations were strongly damped, showing two oscillations within the measurement period compared to the minimum three oscillations for the water-only droplet. Fitting the experimental data to the oscillation damped model, the dampening coefficients for water droplets without and with 0.01 wt% β-aescin were 36 and 58, respectively. The higher dampening coefficient for water + 0.01 wt% β-aescin confirmed that the interfacial shear elasticity was not completely diminished following rupture (yielding) of the interfacial film (to initiate droplet spreading), and the interface remained sufficiently elastic to dampen the bulk oscillation of the droplet. Based on the interfacial rheology data shown in Fig. 4b, the interfacial elasticity during droplet spreading is not thought to result from a rapidly developing interfacial film, but instead from the residual elasticity of the pre-formed film prior to droplet spreading.
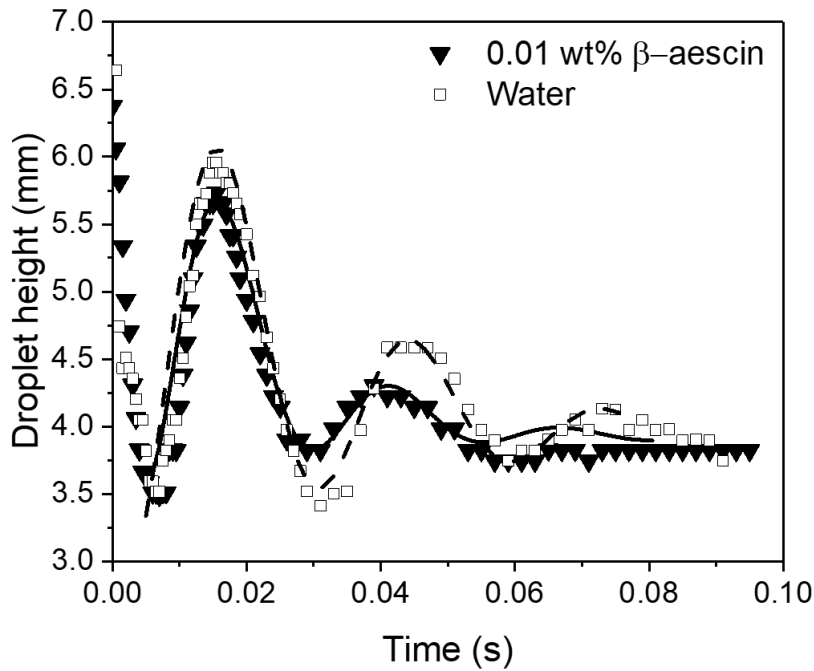
Figure 8. Damped oscillations of detached droplets. Experimental data is shown by the symbols and the damped oscillation model $(A(t) = A_0 exp(-\beta t) \sin(\omega t + \psi))$ represented by the lines (solid and dash).

Free droplet spreading: To verify that the droplet-capillary attachment did not influence the observed enhancement in inertial droplet spreading, the spreading experiments were repeated for free droplets. Free droplets were generated using a 22 G capillary positioned 5.5 mm from the spreading substrate, with droplets detached from the capillary by gently tapping the feed tube to the dispensing capillary. Only droplets with circularity greater than 0.8 at the point of droplet-substrate contact were considered and analyzed. Without β-aescin, all droplets demonstrated a power-law dependency in the region of 0.5 (inertial regime), with the rate of spreading almost independent of the droplet viscosity and surface tension (5 wt% ethanol, 1.5 $\times$ 10^{-3} wt% DG). However, the droplet spreading profile for water + β-aescin was more complex (Fig. 9), a result of the apparent droplet spreading prior to interfacial film rupture (droplet deformation [maximum width / height] at t = 0 (Fig. 9b) and t = 3.2 $\times$ 10^{-3} (interfacial film rupture) (Fig. 9c) was 0.83 and 1.28, respectively). Applying the same analysis method

as previously described, t = 0 was defined as the first contact between the droplet and the substrate. Without β-aescin, all droplets exhibited no resistance to spreading, hence the droplets spread at a rate n′ ~ 0.5. For the water + β-aescin droplet, two decay profiles were observed (boundary at t $\leq$ 3.2 $\times$ 10^{-3}s, Fig. 9a). The slower droplet spreading in Region I was attributed to the balance of hydrodynamic forces and interfacial rigidity, with the interfacial elasticity retarding the outward expanding deformation of the droplet. At t = 3.2 $\times$ 10^{-3} s the β-aescin film yields (droplet deformation = 1.28, Fig. 9c) and the droplet wets the substrate to begin three-phase spreading. In Region II the power-law dependency exceeds all other fluids (n′ = 0.73 $\pm$ 0.02), again confirming that the shear interfacial elasticity of the β-aescin film accelerates the inertial regime of droplet spreading.
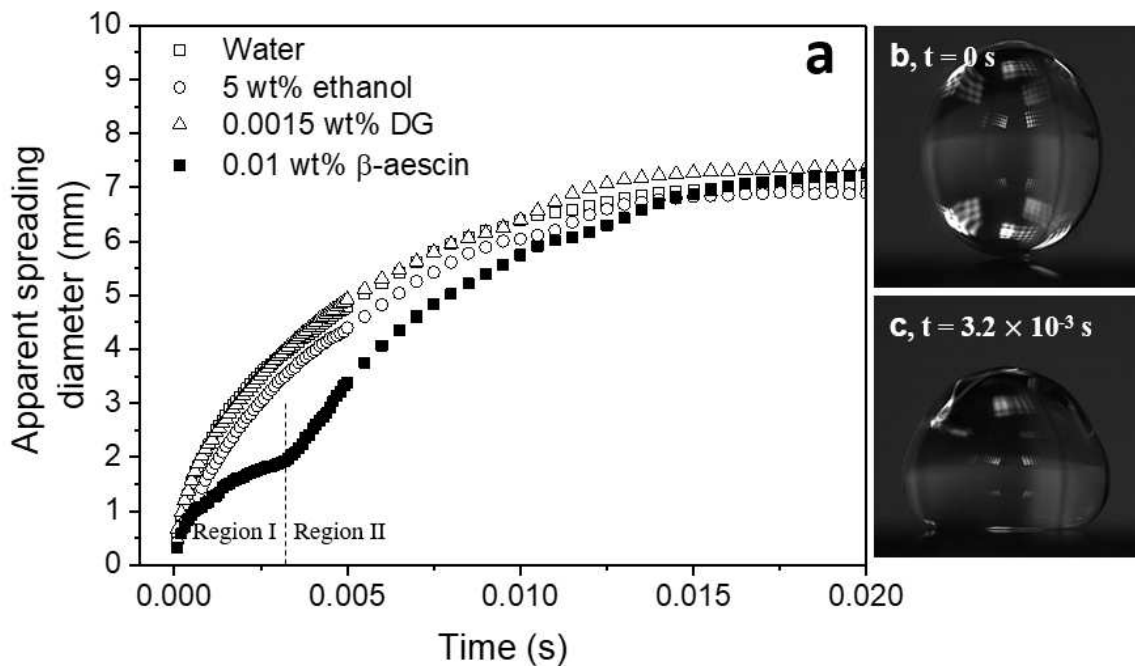

Figure 9. a) Spreading dynamics of free droplets (minimum droplet deformation = 0.8). b) Water + 0.01 wt% β-aescin droplet at substrate contact (t = 0 s), droplet deformation (maximum width / height) = 0.83. c) Maximum droplet deformation (1.28) at interfacial film rupture.

Conclusions

Accelerated droplet spreading in the inertial regime ($n'_1 = 1.05$, $n'_2 = 0.61$) resulted from the yielding of a strongly elastic interfacial film. A concentration of 0.01 wt% β-aescin was shown to significantly increase the interfacial shear elasticity with minimal effect on the bulk fluid (water) viscosity. β-aescin exhibited a molecular area of ~ 0.26 nm^2 with a preferential orientation at the air-water interface being end-on configuration. The high surface excess led to the formation of a strongly elastic interface, with surface shear moduli of 0.57 Pa.m (G') and 0.09 Pa.m (G") after 1 min interfacial aging. The β-aescin stabilized water droplet could significantly deform (degree of deformation = 1.28) before the interfacial film ruptured to promote accelerated droplet spreading in the inertial regime. The residual interfacial elasticity also damped the normal oscillations of a detached droplet, exhibiting only two oscillation cycles as compared to more than three for water-only.

This research has demonstrated the ability to modify the inertial regime of droplet spreading by controlling the interfacial shear rheology. Such control may have desirable implications in many droplet-substrate applications. While the inertial regime of droplet spreading can be manipulated, a similar approach to modify the viscous regime of droplet spreading has not yet been achieved, although one can foresee that such control using surface active species could be highly beneficial.

Author Information

Corresponding Author

D.H.; E: d.harbottle@leeds.ac.uk; T: +44(0)113 343 4154

Supplementary Information

Oscillation strain ramp of an air-water interface stabilized by 0.01 wt% β-aescin following 5 min aging. The yield point was taken to be the crossover point of G' and G'' (indicated by the arrow), Fig. S1.

Acknowledgements

References

1.   de Ruijter, M. J.; De Coninck, J.; Oshanin, G., Droplet Spreading: Partial Wetting Regime Revisited. Langmuir **1999,** 15 (6), 2209-2216.
2.   Vellingiri, R.; Savva, N.; Kalliadasis, S., Droplet spreading on chemically heterogeneous substrates. Physical Review E **2011,** 84 (3), 036305.
3.   Tanner, L., The spreading of silicone oil drops on horizontal surfaces. Journal of Physics D: Applied Physics **1979,** 12 (9), 1473.
4.   Seaver, A. E.; Berg, J. C., Spreading of a droplet on a solid surface. Journal of applied polymer science **1994,** 52 (3), 431-435.
5.   de Gennes, P. G., Wetting: statics and dynamics. Reviews of Modern Physics **1985,** 57 (3), 827-863.
6.   Davis, M. J.; Davis, S. H., Droplet spreading: Theory and experiments. Comptes Rendus Physique **2013,** 14 (7), 629-635.
7.   Sawicki, G., Wetting, Spreading and Adhesion. **1978**.
8.   Eggers, J.; Lister, J. R.; Stone, H. A., Coalescence of liquid drops. Journal of Fluid Mechanics **1999,** 401, 293-310.
9.   Eddi, A.; Winkels, K. G.; Snoeijer, J. H., Short time dynamics of viscous drop spreading. Physics of Fluids **2013,** 25 (1), 013102.
10.   Biance, A.-L.; Clanet, C.; Quéré, D., First steps in the spreading of a liquid droplet. Physical Review E **2004,** 69 (1), 016301.
11.   Bennett, T.; Poulikakos, D., Splat-quench solidification: estimating the maximum spreading of a droplet impacting a solid surface. Journal of Materials Science **1993,** 28 (4), 963-970.
12.   Cazabat, A.; Stuart, M. C., Dynamics of wetting: effects of surface roughness. J. Phys. Chem **1986,** 90 (22), 5845-5849.
13.   Schiaffino, S.; Sonin, A. A., Molten droplet deposition and solidification at low Weber numbers. Physics of Fluids **1997,** 9 (11), 3172-3187.

14.   Lin, P. A.; Ortega, A. In The influence of surface tension and equilibrium contact angle on the spreading and receding of water droplets impacting a solid surface, 13th InterSociety Conference on Thermal and Thermomechanical Phenomena in Electronic Systems, May 30 2012-June 1 2012; 2012; pp 1379-1386.

15.   Chen, L.; Auernhammer, G. K.; Bonaccurso, E., Short time wetting dynamics on soft surfaces. Soft Matter **2011,** 7 (19), 9084-9089.

16.   Stapelbroek, B. B. J.; Jansen, H. P.; Kooij, E. S.; Snoeijer, J. H.; Eddi, A., Universal spreading of water drops on complex surfaces. Soft Matter **2014,** 10 (15), 2641-2648.

17.   Hong, J.; Kim, Y. K.; Kang, K. H.; Oh, J. M.; Kang, I. S., Effects of Drop Size and Viscosity on Spreading Dynamics in DC Electrowetting. Langmuir **2013,** 29 (29), 9118-9125.

18.   McHale, G.; Brown, C.; Sampara, N., Voltage-induced spreading and superspreading of liquids. Nature communications **2013,** 4, 1605.

19.   Bolleddula, D. A. Droplet impact and spreading of viscous dispersions and volatile solutions. University of Washington, 2011.

20.   Bird, J. C.; Mandre, S.; Stone, H. A., Short-time dynamics of partial wetting. Physical review letters **2008,** 100 (23), 234501.

21.   Chen, L.; Bonaccurso, E., Effects of surface wettability and liquid viscosity on the dynamic wetting of individual drops. Physical Review E **2014,** 90 (2), 022401.

22.   von Bahr, M.; Tiberg, F.; Yaminsky, V., Spreading dynamics of liquids and surfactant solutions on partially wettable hydrophobic substrates. Colloids and Surfaces A: Physicochemical and Engineering Aspects **2001,** 193 (1–3), 85-96.

23.   Svitova, T.; Hill, R. M.; Radke, C. J., Adsorption layer structures and spreading behavior of aqueous non-ionic surfactants on graphite. Colloids and Surfaces A: Physicochemical and Engineering Aspects **2001,** 183–185, 607-620.

24.   Roques-Carmes, T.; Mathieu, V.; Gigante, A., Experimental contribution to the understanding of the dynamics of spreading of Newtonian fluids: Effect of volume, viscosity and surfactant. Journal of colloid and interface science **2010,** 344 (1), 180-197.

25.   Winkels, K. G.; Weijs, J. H.; Eddi, A.; Snoeijer, J. H., Initial spreading of low-viscosity drops on partially wetting surfaces. Physical Review E **2012,** 85 (5), 055301.

26.   Liang, Z.-P.; Wang, X.-D.; Lee, D.-J.; Peng, X.-F.; Su, A., Spreading dynamics of power-law fluid droplets. Journal of Physics: Condensed Matter **2009,** 21 (46), 464117.

27.   Rafaı, S.; Sarker, D.; Bergeron, V.; Meunier, J.; Bonn, D., Superspreading: aqueous surfactant drops spreading on hydrophobic surfaces. Langmuir **2002,** 18 (26), 10486-10488.

28.   Dutschk, V.; Breitzke, B., Spreading characteristics of aqueous surfactant solutions on polymer surfaces. Tenside Surfactants Detergents **2005,** 42 (2), 82-87.

29.   Dutschk, V.; Breitzke, B.; Grundke, K., Wetting of aqueous surfactant solutions on polymer surfaces. Tenside, surfactants, detergents **2003,** 40 (5), 250-255.

30.   Starov, V. M.; Kosvintsev, S. R.; Velarde, M. G., Spreading of Surfactant Solutions over Hydrophobic Substrates. Journal of Colloid and Interface Science **2000,** 227 (1), 185-190.

31.   Kuznicki, N. P.; Harbottle, D.; Masliyah, J.; Xu, Z., Dynamic Interactions between a Silica Sphere and Deformable Interfaces in Organic Solvents Studied by Atomic Force Microscopy. Langmuir **2016,** 32 (38), 9797-9806.

32.   Kuznicki, N. P.; Harbottle, D.; Masliyah, J. H.; Xu, Z., Probing Mechanical Properties of Water–Crude Oil Interfaces and Colloidal Interactions of Petroleum Emulsions Using Atomic Force Microscopy. Energy & Fuels **2017,** 31 (4), 3445-3453.

33.   Bi, J.; Yang, F.; Harbottle, D.; Pensini, E.; Tchoukov, P.; Simon, S. b.; Sjöblom, J.; Dabros, T.; Czarnecki, J.; Liu, Q., Interfacial layer properties of a polyaromatic compound and its role in stabilizing water-in-oil emulsions. Langmuir **2015,** 31 (38), 10382-10391.

34.   Harbottle, D.; Chen, Q.; Moorthy, K.; Wang, L.; Xu, S.; Liu, Q.; Sjoblom, J.; Xu, Z., Problematic stabilizing films in petroleum emulsions: Shear rheological response of viscoelastic asphaltene films and the effect on drop coalescence. Langmuir **2014,** 30 (23), 6730-6738.

35.   Bonn, D.; Eggers, J.; Indekeu, J.; Meunier, J.; Rolley, E., Wetting and spreading. Reviews of modern physics **2009,** 81 (2), 739.

36.   Kovalchuk, N. M.; Barton, A.; Trybala, A.; Starov, V., Surfactant Enhanced Spreading: Catanionic Mixture. Colloids and Interface Science Communications **2014,** 1, 1-5.

37.   Leiske, D. L.; Monteux, C.; Senchyna, M.; Ketelson, H. A.; Fuller, G. G., Influence of surface rheology on dynamic wetting of droplets coated with insoluble surfactants. Soft Matter **2011,** 7 (17), 7747-7753.

38.   Golemanov, K.; Tcholakova, S.; Denkov, N.; Pelan, E.; Stoyanov, S. D., Remarkably high surface visco-elasticity of adsorption layers of triterpenoid saponins. Soft Matter **2013,** 9 (24), 5738-5752.

39.   Pekdemir, T.; Ishigami, Y.; Uchiyama, H., Characterization of aescin as a biosurfactant for environmental remediation. Journal of Surfactants and detergents **1999,** 2 (3), 337-341.

40.   Yeung, A.; Dabros, T.; Masliyah, J., Dissipative Interfaces and Departures from the Young−Laplace Equation. Langmuir **1997,** 13 (24), 6597-6606.

41.   Stanimirova, R.; Marinova, K.; Tcholakova, S.; Denkov, N.; Stoyanov, S.; Pelan, E., Surface rheology of saponin adsorption layers. Langmuir **2011,** 27 (20), 12486-12498.

42.   Zhang, H.; Yu, K.; Cayre, O. J.; Harbottle, D., Interfacial Particle Dynamics: One and Two Step Yielding in Colloidal Glass. Langmuir **2016,** 32 (50), 13472-13481.

43.   Lorent, J. H.; Quetin-Leclercq, J.; Mingeot-Leclercq, M.-P., The amphiphilic nature of saponins and their effects on artificial and biological membranes and potential consequences for red blood and cancer cells. Organic & biomolecular chemistry **2014,** 12 (44), 8803-8822.

44.   Ata, S., The detachment of particles from coalescing bubble pairs. Journal of colloid and interface science **2009,** 338 (2), 558-565.